# IDENTIFICATION OF THE FLAME DESCRIBING FUNCTION OF A PREMIXED SWIRL FLAME FROM LES

**H.J. Krediet*, C.H. Beck*, W. Krebs*, S. Schimek**, C.O. Paschereit****

e-mail of corresponding author: harmen.krediet@siemens.com

*Siemens AG, Fossil Power Generation, Mellinghoferstr. 55, 45473 Mülheim an der Ruhr, Germany

**Chair of Fluid Dynamics, Hermann-Föttinger-Institute, Technische Universität Berlin, Germany

## Abstract

Thermoacoustic characterization of gas turbine combustion systems is crucial for a successful development of new gas turbine engines to meet emission and efficiency targets. In this context, it becomes more and more necessary to predict the limit cycle amplitudes of thermoacoustic induced combustion instabilities to figure out if they can be tolerated or if they are above the critical design limit and will cause damage to the engine. For the prediction of limit cycle amplitudes, the nonlinear flame response of the combustion system is needed, which is represented in this work by the Flame Describing Function (FDF). In this paper, the identification of the FDF from a Large Eddy Simulation (LES) is validated. The test case used was a premixed atmospheric swirl flame, for which experimental data on the FDF was available. First a steady reacting LES solution was obtained and compared to experimental data. The simulation was then excited by superimposing a mono-frequency harmonic wave on the velocity inlet boundary condition. Both the frequency and amplitude of the acoustic wave were varied to obtain the FDF. The calculated FDF was in good agreement with experimental data. At a frequency of 115 Hz, the flame was found to saturate for larger excitation amplitudes. A detailed analysis of the LES results revealed that local quenching of the flame is the root cause leading to this saturation.

## I. Introduction

In order to meet low NOx emission targets for modern gas turbines used for power generation, lean premixed combustion technology needs to be applied. A drawback of this combustion technology is that the resulting high power density makes these combustion systems prone to thermo-acoustic oscillations, limiting the operational envelope of the gas turbine. These oscillations arise from the interactions between the acoustics of the combustion system and the heat released by the flame. The general implications of this feedback cycle to gas turbine combustors have been outlined in several works, such as those by Dowling et al. [1] and Krebs et al. [2].

In the design phase of a gas turbine combustor, it is desirable to predict the stability behavior over the whole operational envelope. State of the art models [2-4] predict excited frequencies and presence of instability with fair accuracy. However, gas turbine manufacturers also require the knowledge of the limit cycle amplitude of the pressure oscillations, since it is this quantity which determines the operational envelope of these engines.

A commonly used quantity in thermo-acoustic modeling is the Flame Transfer Function (FTF), which gives the heat release rate of the flame in response to acoustic fluctuations from a reference position upstream of the flame. The FTF's can be used as inputs to low order thermo-acoustic system models, which are then solved to determine the excited frequencies (via eigenfrequencies and growth rates) of a given combustion system. However, FTF's cannot predict the limit cycle amplitude, as the limit cycle amplitudes are governed by nonlinear effects.

Currently, the heat release rate of the flame is considered the most dominant nonlinear term for gas turbine engines in power generation [5-8]. The nonlinear system can be explained using Figure 1. This figure shows the energy of a system as a function of the perturbation level, represented by the square of the acoustic velocity. It can also be seen in the figure that the amplitude of a limit cycle is governed by a balance of energy gain and losses. In this case the acoustic losses present in the combustion system, such as losses through the boundaries and by turbulence (represented by the dashed line), are assumed to be linear [8-9]. The flame dynamics (represented by the solid line), however, have a linear regime for smaller perturbation amplitudes (region I) as well as a nonlinear regime for larger perturbation amplitudes (region 'II'). For linear losses and nonlinear gains, it can be seen that the acoustic energy would increase unbounded in region I since no equilibrium point can be reached. However, it is apparent that a stable limit cycle can be sustained within the nonlinear region.

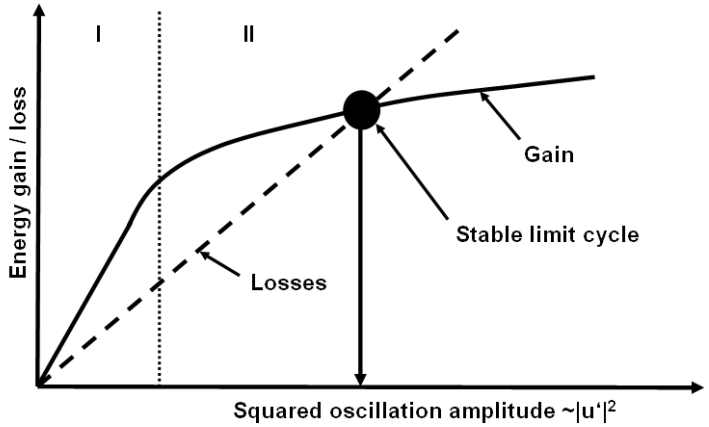


**Figure 1**. Interaction between energy losses and energy gain via unsteady heat addition.

One of the reasons for this nonlinear flame saturation is that the acoustic velocity can become of the same order of magnitude as the mean flow [5-9], which can lead to local extinction of the flame. Modeling such physics requires a nonlinear model for the flame unsteadiness. The standard Flame Transfer Function is a linear model and only describes the physics in region 'I' of the figure. A common nonlinear modeling approach, originally introduced by Dowling [9], is to 'upgrade' the FTF to the so-called Flame Describing Function (FDF):

$$\frac{Q'}{Q_0} = FDF(\omega, u'_{rms})\frac{u'}{u_0} \tag{1}$$

Here, $Q_0$ and Q' represent the mean heat release by the flame and its fluctuation, $u_0$ and u' represent the mean and acoustic velocity, $\omega$ is the frequency and $u'_{rms}$ stands for the root mean square acoustic velocity. Key references for measurements of the nonlinear heat release rate of various premixed flames include Ref 5-9. The main findings of these authors was that the Flame Describing Function, and thus the heat release rate by the flame, decreases for increasing velocity amplitudes, as depicted in Figure 1. Importantly, it was also found that the acoustic limit cycle pressure amplitudes were an order of magnitude smaller than the mean pressure. For example, Lieuwen et. al. [6] measured pressure amplitudes of up to 2% of the mean pressure, thus justifying the treatment of the acoustics themselves as linear.

Currently, most work on Flame Describing Functions has been experimental. Several works describe the identification of the linear Flame Transfer Function by numerical methods, especially CFD [10-11]. In the state of the art procedure, the FTF is determined by Large Eddy Simulations where the flame is excited by perturbing the boundaries of the combustor

using a broadband frequency signal [11]. The work on determining FDF's from CFD on the other hand is very limited. Armitage et al. [12] investigated the FDF for a two dimensional ethylene flame, which was close to laminar, using a URANS approach. For highly turbulent flows no such investigation has, to the knowledge of the author, been performed so far.

The main objective of this paper is to validate the identification of the Flame Describing Function (FDF) from Large Eddy Simulation. The flame saturation mechanism will be studied as well. A turbulent premixed swirl stabilized combustor was chosen for this study. Experimental data is available for this setup and was used to compare against the simulations. In the following section the test case will be described. Next, the CFD setup is discussed, followed by a comparison between numerical and experimental data.

## II. Description of test case

The test case used was an atmospheric swirl-stabilized premixed flame. The test rig is located at the Chair of Fluid Dynamics at the University of Berlin. All experimental data was obtained by Schimek et al. [13-14]. In Figure 2 a schematic drawing of the rig is shown.

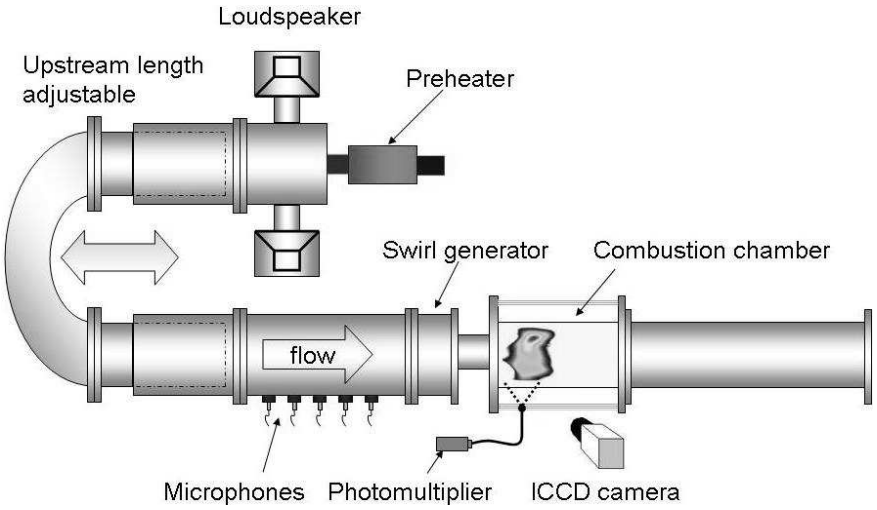


**Figure 2.** Schematic drawing of the test rig

The burner consists of a swirl generator followed by an annular duct and an area discontinuity to the combustion chamber. After passing the swirler, the flow enters an annular duct, followed by an area expansion to the combustion chamber where a vortex breakdown is established. This leads to a recirculation zone and thus to a stabilization of the flame.

The air is preheated upstream of the swirl generator to 220°C. Four speakers are mounted in the upstream duct, providing the acoustic forcing. The length of the upstream section could be varied in order to create resonance. This was required to achieve the required excitation amplitudes at specific frequencies. The setup is able to excite the acoustic velocity at the flame with amplitudes of up to 100% of the mean flow velocity.

The setup was both run in technically premixed and fully premixed mode. For technically premixed combustion operation, fuel (natural gas) is injected through sixteen fuel nozzles located in the swirl generator. For the perfectly premixed operation, air and fuel were mixed far upstream of the swirler.

The heat release rate of the flame was measured using OH* chemiluminescence. Upstream of the swirl generator, an array of microphones has been mounted. The acoustic field was determined from these microphones using the multi-microphone-method. Schimek et al. both modeled and measured the transfer matrix of the swirl generator [13], making it

possible to calculate the velocity fluctuation at the combustion chamber inlet based on the acoustic field upstream of the swirl generator.

The Flame Describing Function is available for different operating conditions (swirl numbers, air mass flows, preheat temperature, equivalence ratio) and for the technically and perfectly premixed operating points. In the CFD analysis, the focus was on the perfectly premixed mode. For perfectly premixed combustion, the relation between heat release fluctuations (Q') and OH* fluctuations is commonly assumed to be linear. The advantage of modeling the perfectly premixed mode is that Q' can be assumed to be proportional to OH*. The formation of OH* is not directly predicted by the CFD code.

Measurement data are available for different swirl numbers, air mass flows, preheat temperature and equivalence ratio. In Table 1 the parameters for the operating point investigated in the CFD analysis are shown.

**Table 1.** Investigated operating point

| Operating Mode | Perfectly premixed |
|---|---|
| Swirl number | 1.2 |
| Air mass flow | 0.0417 kg / s |
| Air preheat temperature | 220°C |
| Equivalence ratio | 0.65 |

## III. CFD Setup

To be able to accurately resolve all important physical phenomena that may influence the nonlinear behavior of the flame, a Large Eddy Simulation was performed. The configuration was calculated using a Siemens in-house developed reacting LES code, which is an extension of the open source LES code OpenFoam. The LES fully resolves the large turbulent structures, but only models the subscale turbulence. In this case, the Smagorinsky sub grid model was used, which models the sub grid viscosity $\mu_{SGS}$ as:

$$\mu_{SGS} = \bar{\rho}(C_S\Delta)^2\left|\tilde{S}\right|, \quad \text{with} \quad \tilde{S}_{ij} = \frac{1}{2}\left(\frac{\partial\tilde{u}_i}{\partial x_j} + \frac{\partial\tilde{u}_j}{\partial x_i}\right) \tag{2}$$

Here, $\bar{\rho}$ is the filtered density, $C_S$ a model constant ($C_S = 0.2$), $\Delta$ the sub grid filter width and $\tilde{u}$ the velocity. The combustion process is modeled using the Turbulent Flamespeed Closure model (TFC). The model solves a transport equation for the filtered reaction progress variable $\tilde{c}$, which is a scalar that takes values between 0 and 1. For fresh gasses, $\tilde{c} = 0$, and for burned gasses, $\tilde{c} = 1$.

$$\frac{\partial(\bar{\rho}\,\tilde{c})}{\partial t} + \frac{\partial(\bar{\rho}\,\tilde{u}_i\,\tilde{c})}{\partial x_i} = \frac{\partial^2}{\partial x_i \partial x_i}\left(\bar{\rho}\bar{D} + \frac{\mu_T}{S_C}\,\tilde{c}\right) + \bar{\rho}\tilde{\omega}_R \tag{3}$$

Here, $\bar{D}$ is the laminar diffusivity, $\mu_T = \mu_0 + \mu_{SGS}$ the effective turbulent viscosity and $S_C$ the turbulent Schmidt number. In the TFC, the concept of the laminar flame speed $S_L$ is extended to its turbulent form. The chemical source term $\bar{\rho}\tilde{\omega}_R$ is:

$$\overline{\rho}\widetilde{\omega}_R = \overline{\rho}_u S_T \left|\nabla \widetilde{c}\right| = \overline{\rho}_u S_L \Sigma \left|\nabla \widetilde{c}\right| \tag{4}$$

Here $\overline{\rho}_u$ is the density of the unburned gas and $\Sigma$ is the sub grid scale wrinkling factor (the ratio between the turbulent and laminar flame speed). The specific model for the wrinkling factor that was used in the current work was developed by Bradley [15]. The algebraic model for the turbulent burning velocity is based on an experimental data set.

$$\Sigma = 1 + A / Le \left( \frac{u'_{SGS}\ l_T}{\alpha_u} \right)^{0.5} \tag{5}$$

The value of the constant A is 0.5, $Le$ is the Lewis number and $u'_{SGS}$, $l_T$ and $\alpha_u$ are the sub grid velocity, length scale and thermal diffusivity respectively. The unstrained laminar flame speed $S_L$ is obtained using a one-dimensional premixed flame computation. However the true flame speed is reduced (the flame is quenched) by effects of strain and heat losses. To account for this, the following model, which is based on the model of Tay et al. [16], was used:

$$\frac{S_{L,strained}}{S_{L,unstrained}} = (1 - Ma^* \ln(1 + Ka)) \exp(-Ka\ \chi) \tag{6}$$

Where (7)

$$Ka = \frac{\alpha \kappa}{S_{L,unstrained}^{\ 2}} \qquad \beta = \frac{T_{ad} - T_{loss} - T_u}{T_{ad} - T_u}$$

$$\chi = \frac{Ze}{2} \frac{1-\beta}{\beta^3} \qquad Ze = \frac{E_a}{2T_{ad}^2} (T_{ad} - T_u)$$

In this model, κ is the strain rate and $Ma^*$ is a model parameter which is obtained by fitting the outlined model to results from a 1D counter flow simulation for a range of heat loss numbers β and Karlovitz numbers Ka. The exact procedure is described by Tay et al [16]. The other parameters are dimensionless numbers and are defined above. This model improves the calculation of the turbulent flame speed in regions of large shear and regions close to walls where non-adiabatic conditions prevail. The implementation of the combustion and quenching model in OpenFoam was validated by di Domenico et al. [17].

In Figure 3 the computational grid is shown as well as a more detailed view of the swirl generator. The grid was generated with OpenFoam's mesh generator, SnappyHexMesh. It consists of approximately 3.7 million hexahedral cells and contains the full 360° burner geometry. It can be seen that regions with varying mesh density are specified. This way the most important parts of the geometry are accurately resolved, while the less critical sections do not require as many cells. The upstream section with the loudspeakers was not fully modeled, but the CFD Model starts 30 cm upstream of the swirl generator. It was assumed that the flow is one-dimensional at this location.

In the simulation, nonreflecting boundary conditions were used for the velocity, pressure, and temperature at the inlet and outlet, which assured that acoustic waves leave the domain. The walls of the combustor are assumed to have a constant temperature of 800 K. This is indicated in Figure 3 as well. The exact temperature of the wall is not known, but this

estimation will be closer to the actual temperature than it would be if adiabatic walls were used. It was shown by Tay et al. [11] that the modeling of heat losses through the walls is very important for accurate predictions of the heat release distribution, and thus of the predicted flame transfer functions. The inclusion of these heat losses results in a longer flame and a larger phase between velocity and heat release fluctuations.

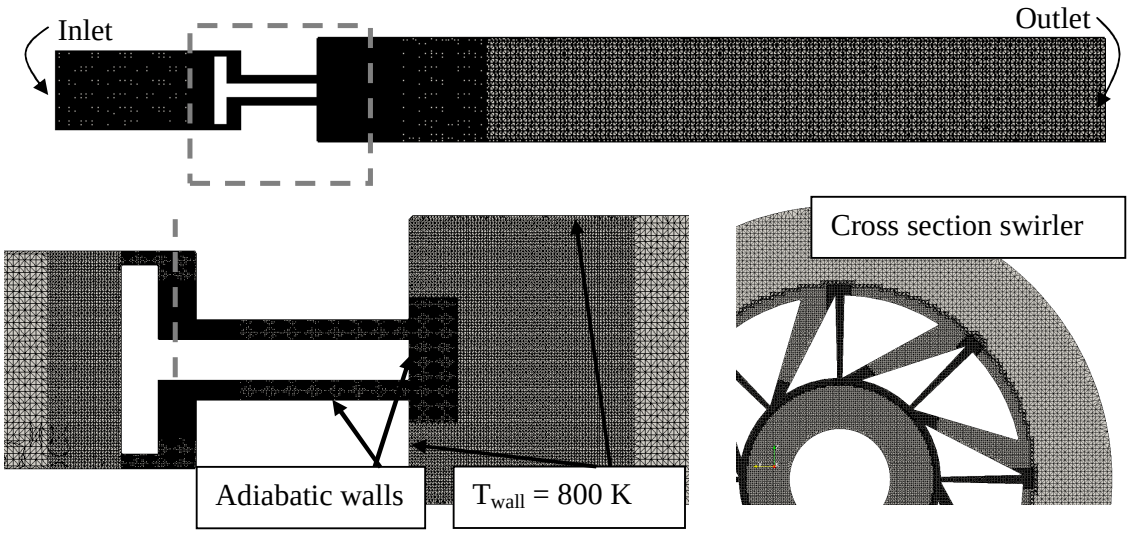


**Figure 3.** Grid and boundary conditions

Both the spatial and temporal derivatives were discretizised using 2nd order discretization schemes. A fixed time step of dt=5e-7 s was chosen, assuring that the acoustic CFL number is smaller than 0.7. This guarantees both robustness of the simulation and negligible dissipation of acoustic waves.

In the present work, first a LES without excitation was performed. After obtaining a converged reacting LES, mono-frequency harmonic excitation was used for the perturbation of the velocity at the inlet. Frequencies below 60 Hz could not be used because the non reflecting boundary conditions act like low-pass filters and frequencies below 60 Hz were still in the reflective range. All frequencies larger than 60 Hz are reflected less than 10% at the inlet and exit. The inlet velocity has the following form:

$$\vec{u}(\vec{x},t)\,|_{inlet} = \vec{u}_{mean}(\vec{x})\left[1 + A\sin(2\pi f_i t)\right] \tag{8}$$

Here $f$ is the frequency and A the amplitude of the acoustic wave. Both have been varied in this study. To obtain the Flame Describing Function, time series of the velocity upstream of the flame (area averaged over the annular duct) and the volume integrated heat release by the flame have been sampled.

The acoustic velocity and heat release are both normalized by their mean values. The Flame Describing Function at a certain frequency and amplitude has finally been calculated by taking the Fourier Transform (FFT) of the time series:

$$FDF(\omega, u'_{rms}) = \frac{fft(Q'/Q_0)}{fft(u'/u_0)} \tag{9}$$

## IV. Results of the simulation without excitation

In Figure 4 the time-averaged velocity field can be seen. The bottom part of the figure shows a contour plot of the magnitude of velocity, while the top part shows a vector plot. Both an outer recirculation zone in the corner of the combustion chamber and a strong inner recirculation zone were observed in the simulations. These have been indicated in the figure as well. The time-averaged velocity field is compared against PIV measurements in Figure 5.

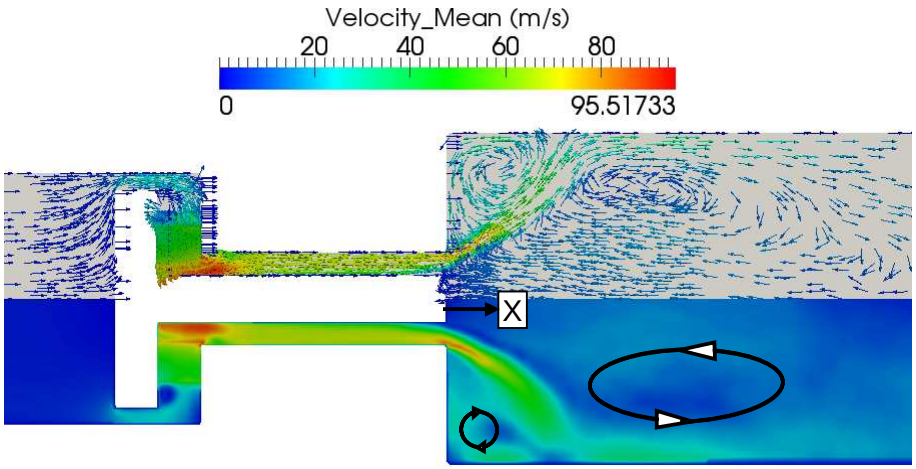


**Figure 4.** Mean velocity field inside the combustion chamber, averaged over 40 ms

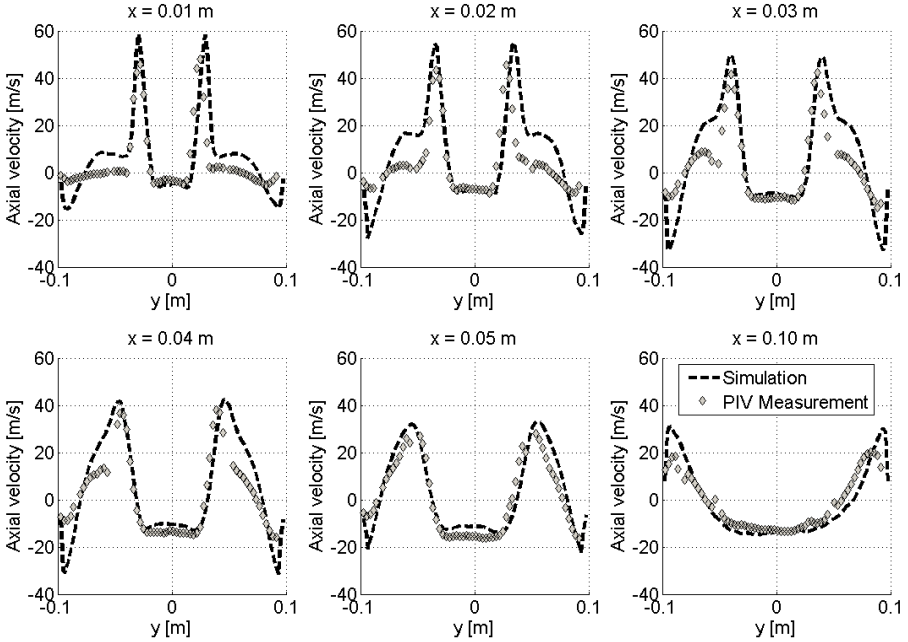


**Figure 5.** Comparison of predicted mean axial velocity against PIV Measurement

The flow field is compared at different axial locations, where the coordinate 'x" represents the distance from the inlet of the combustion chamber (as indicated in Figure 4). The simulation generally shows good agreement with the measurements. The location and magnitude of the peak velocities are well predicted, as well as the central recirculation zone. The velocity close to the walls of the combustor is over predicted in the simulation, especially for $x < 0.05$ m. According to the University of Berlin, there may be some measurement inaccuracy close to the walls due to contamination of the windows. Another reason for this

may be the wall law used by the LES turbulence model. This will be investigated in more detail in future work.

The radial component of the velocity field was compared against PIV as well but is not shown in this paper. Also for the radial velocity, the peak values and central recirculation zone are well predicted, but there is some over prediction in the outer recirculation zone.

The instantaneous temperature field is shown in Figure 6. A contour of the reaction progress variable ($\tilde{c} = 0.9$) has been added to the figure as well to indicate the location of the flame front. It can be seen that the combustion process already starts in the annular tube. When looking at the velocity profile (Figure 4), it can also be seen that the flow detaches from the walls, most likely due to the large swirl number.

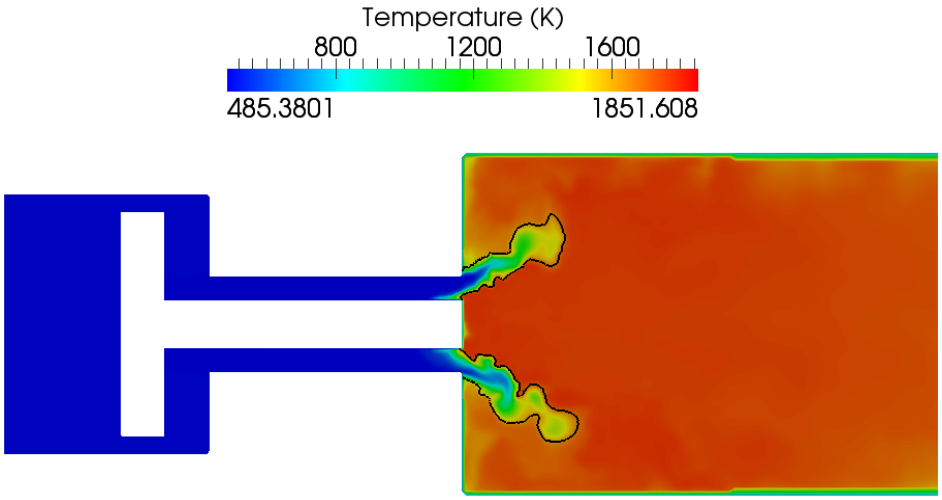


**Figure 6.** Instantaneous temperature field inside the combustion chamber. Black line represents an isocontour of the reaction progress variable ($\tilde{c} = 0.9$).

## V. Results of the simulation with excitation

In Figure 7 an example of a typical time series of the velocity perturbation upstream of the flame and the volume integrated heat release can be seen. The example shows the response at 115 Hz and an acoustic velocity with an amplitude equivalent to 10% of the mean flow velocity. Both quantities have been normalized by there mean values. With the harmonic excitation, clearly a phase difference and a difference in amplitude can be seen between velocity and heat release.

For each harmonic simulation the amplitude and phase of the FDF are determined according to equation 9. In Figure 8 the measured and simulated FDF are compared. Measurement data is available for 7 different excitation amplitudes ($u'/u_0 = 0.1, 0.2, 0.3, 0.4, 0.5, 0.6, 0.7$) but only the data for $u'/u_0$ equal to 0.1, 0.4 and 0.7 is shown. For the excitation level $u'/u_0 = 0.1$, six distinct frequencies have been simulated. For the larger excitation amplitudes, only simulations at 115 and 258 Hz have been done so far. The simulated frequencies and amplitudes are given in the figure.

The simulations generally agree well with the measurements. The amplitude of the FDF is very well predicted, especially for frequencies larger than 150 Hz. The maximum amplitude of the FDF is predicted at 115 Hz but at a slightly lower value than the measurement. At the frequency of 115 Hz, simulations at 3 amplitudes have been done. It can be seen that the amplitude of the FDF reduces for the larger excitation amplitudes. This means that the

response of the flame weakens for larger velocity amplitudes, which is the phenomenon sketched in Figure 1. From this it can be concluded that the nonlinear saturation of the flame is captured by the simulation. Also a simulation at 258 Hz and $u'/u_0 = 0.4$ has been done. For this frequency the flame does not show any saturation in simulation and experiment for the excitation amplitudes considered.

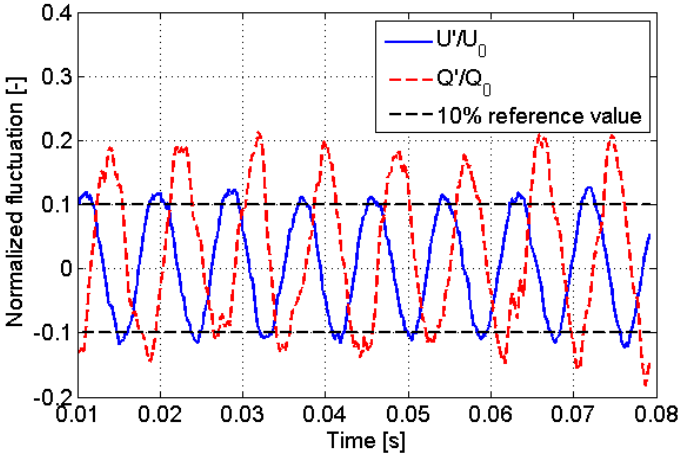


**Figure 7.** Example of sampled acoustic velocity at burner exit and heat release. Both quantities are normalized by their mean values.

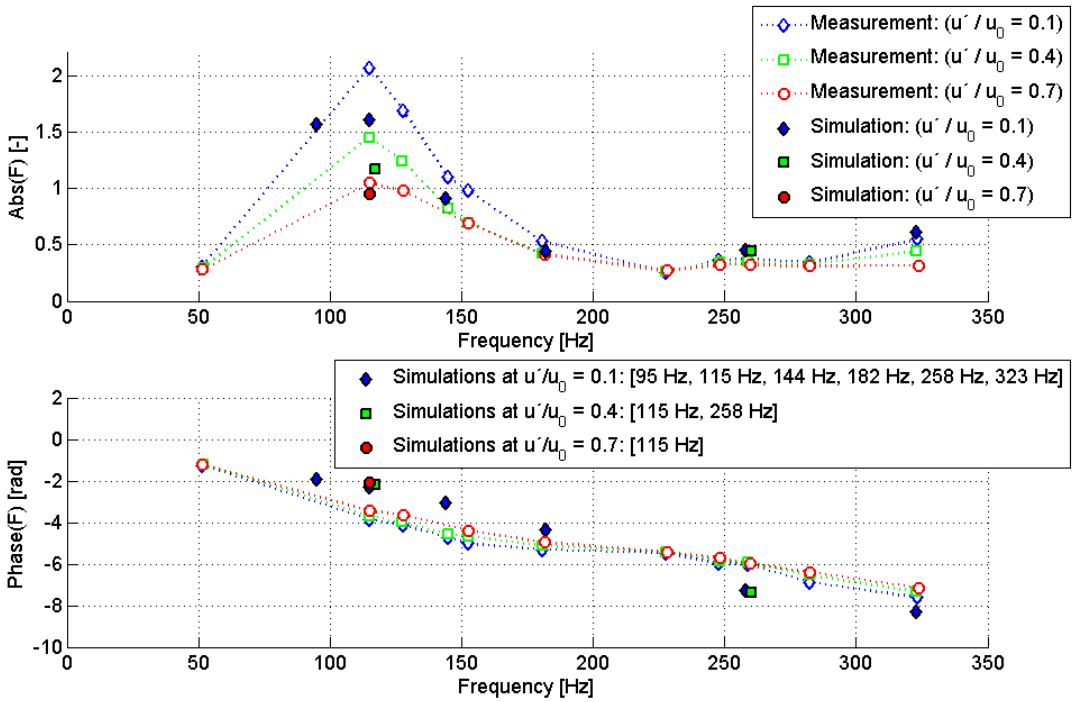


**Figure 8.** Comparison of measured and simulated Flame Describing Function.

In the measurements, also a minimum gain was found at approximately 50 Hz. The frequency at 50 Hz has not been simulated. The reason for this is that at this frequency, as explained in section III, there is considerable reflection of acoustic waves at the inlet and exit. Furthermore the CPU time of a simulation with harmonic excitation is inversely proportional to the frequency, which would make this a very expensive calculation.

When looking at the phase plot, for frequencies below 200 Hz it is slightly under predicted, whereas the phase is slightly over predicted for the larger frequencies. Nonetheless, the general agreement between measurements and simulation is good. The phase decreases approximately linearly with frequency, which indicates that the flame has a constant time lag (in this case $\tau$ = 3.95 ms). The phase was did not appear to be dependent on the excitation amplitudes, both in simulation and experiments.

In

Figure **9** the saturation of the flame is investigated in more detail. This investigation is done for a frequency of 115 Hz, where strong saturation at larger excitation amplitudes was observed. The figure shows isosurfaces of the reaction progress variable ($\tilde{c} = 0.9$), which are assumed to be a good indication of the flame surface. The isosurfaces have been colored by the strain rate, which was calculated as $\kappa = 2 / 3 \nabla \cdot \tilde{u}$. For each excitation amplitude, an isosurface is shown during a part of the acoustic cycle where the heat release (normalized) was increasing ($dQ/dt > 0$) and during a part of the acoustic cycle where the heat release was decreasing ($dQ/dt < 0$).

It can be seen that during the part of the cycle with $dQ/dt > 0$ the flame has a compact surface for all excitation amplitudes. During the part of the cycle with $dQ/dt < 0$ it can be seen that the flame does not have a compact surface for the larger excitation amplitudes. This suggests that the flame is partly quenched. At $u'/u_0 = 0.7$ this can be seen most clearly. In the measurements, local flame quenching was also found to be the saturation mechanism [14].

The strain rate can obtain large values up to 15000 1/s for the largest excitation amplitude. This leads to the hypothesis that the reason that the flame quenches for larger amplitudes is related to the large strain rates during part of the acoustic cycle. This hypothesis will be further evaluated in future work.

## VI. Conclusions and recommendations

From the comparison between simulations and experiments, it can be concluded that the Flame Describing Function can successfully be predicted using Large Eddy Simulations. The saturation of the flame at a frequency of 115 Hz, which was observed during the measurements, was also predicted using LES. At a frequency of 258 Hz, no noticeable saturation was found in either the experiments or simulation.

An investigation of the flame front surface and the strain rate on this surface led to the conclusion that flame quenching (local extinction) is likely the mechanism leading to this saturation. The large strain rates observed during part of the acoustic cycle lead to the hypothesis that this local flame quenching is caused by strain. This hypothesis will be investigated and quantified in more detail in future work.

Now that the Flame Describing Function is known both from measurements and simulations, it will be used as input for a nonlinear low order thermo-acoustic system model. With this system model, the limit cycle pressure amplitude will be predicted and compared with experimental data. These results will be presented in future work.

All data points for the Flame Describing Function so far have been determined using mono-frequency harmonic excitation, while the post processing methods for broad band excitation only work for small excitation amplitudes (linear regime). However, harmonic excitation has the disadvantage that it requires large computational efforts. In future work, it could be investigated if it is possible to extend the method with broadband excitation to the nonlinear range.

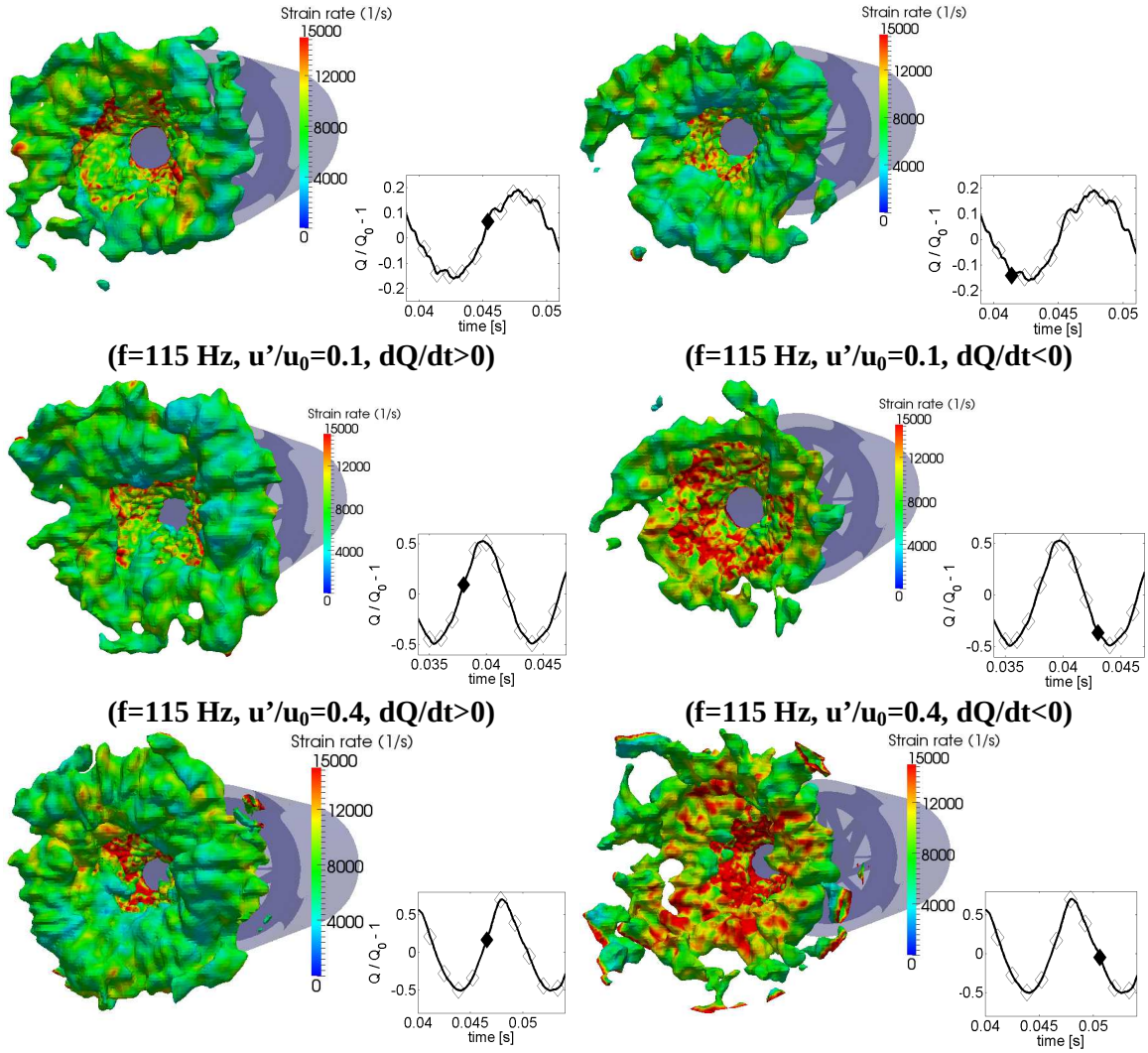


**Figure 9.** Isosurface of the reaction progress variable ($\tilde{c} = 0.9$) during a period of oscillation. Isosurface is coloured by the strain rate

**Acknowledgments**

The authors would like to acknowledge the funding of this research by the EC in the Marie Curie Actions – Networks for Initial Training program, under call FP7-PEOPLE-2007-1-1-ITN, Project LIMOUSINE with project number 214905 and by the Research Association for Combustion Engines (FVV), Project 923 - Nonlinear flame transfer functions. Special thanks go to CERFACS for providing access to their computing resources, which made the calculations that are presented in this paper possible.

**References**


[1] Dowling, A.P., and Stow, S.R., "Acoustic analysis of gas turbine combustors", *Journal of Propulsion and Power* 19(5):751-763 (2003)

[2] Krebs, W., Flohr, P., Prade, B. and Hoffmann, S., "Thermoacoustic Stability Chart for High Intense Gas Turbine combustion Systems", *Combustion Science & Technology* 174: 99–128 (2002)

[3] Kim, K.T., Lee, H.J., Lee, J.G., Quay, B. and Santavicca, D., "Flame transfer function measurement and instability frequency prediction using a thermo acoustic model", *Proc ASME Turbo Expo*, Orlando (2009)

[4] Velluci, V., Schuermans, B., Nowak, D., Flohr, P. and Paschereit, C.O., "Thermoacoustic modeling of a gas turbine combustor equipped with acoustic dampers", *Proc ASME Turbo Expo*, Vienna (2004)

[5] Balachandran, R., Ayoola, B.O., Kaminski, C.F., Dowling, A.P., and Mastorakos, E., "Experimental investigation of the nonlinear response of turbulent premixed flames to imposed inlet velocity oscillations", *Combustion and Flame* 143:37-55 (2005)

[6] Lieuwen, T. and Neumair, Y., "Nonlinear pressure-heat release transfer function measurements in a premixed combustor", *Proc Combustion institute*, 29:99-105 (2002)

[7] Lieuwen, T., Bellows, D., Bobba, M.K. and Seitzman, J.M., "Nonlinear Flame transfer function characteristics in a swirl stabilized combustor", *Transactions ASME* 129:954-961 (2007)

[8] Dowling, A. P and Stow, S. R., "A time-domain network model for nonlinear thermo-acoustic oscillations", *Proc ASME Turbo Expo*, Berlin (2008)

[9] Dowling, A.P., "Nonlinear self-excited oscillations of a ducted flame", *Journal of Fluid Mechanics* 346: 271-290 (1997)

[10] Armitage, C.A., Riley, A.J., Cant, R.S., Dowling, A.P., and Stow, S.R., "Flame transfer function for swirled LPP combustion from experiments and CFD", *Proc ASME Turbo Expo*, Vienna (2004)

[11] Tay Wo Chong, L., Komarek, T., Kaess, R., Föller, S. and Polifke, W., "Identification of Flame Transfer Functions from LES of a premixed swirl burner", *Proc of ASME Turbo Exp*, GT2010-22769, Glasgow (2010)

[12] Armitage, C.A., Balachandran, R., Mastorakos, E. and Cant, R.S., "Investigation of the nonlinear response of turbulent premixed flames to imposed inlet velocity oscillations", *Combustion and Flame* 146:419-436 (2006)

[13] Schimek, S., Moeck, J.P., Paschereit, C.O., "Design of a combustion test rig with high amplitude forcing capabilities for nonlinear flame transfer function measurements", *Proc ICSV 16*, Krakow, Poland (2009)

[14] Schimek, S., Moeck, J.P., Paschereit, C.O., "An experimental investigation of the nonlinear response of an atmospheric swirl-stabilized premixed flame", *Proc of ASME Turbo Expo*, GT2010-2282, Glasgow (2010)

[15] Bradley, D. 1992. "How fast can we burn?", *Twenty-Fourth Symposium (International) on Combustion*, pp 247-262 (1992)

[16] Tay Wo Chong, L., Komarek, T., Zellhuber, M., Lenz, J., Hirsch, C. and Polifke, W., "Influence of strain and heat loss on flame stabilization in a non-adiabatic combustor", *European combustion meeting* (2009)

[17] Di Domenico, M., Beck, C.H., Lammel, O, Krebs, W. and Noll, B., "Experimental and numerical investigation of turbulent, lean, high-strained, confined, jet flames", *Proc 49th AIAA Aerospace Sciences Meeting*, Orlando (2011)

[18] Palies, P., Schuller, T., Durox, D. and Candel, S., "The combined dynamics of swirler and turbulent premixed swirling flames", *Combustion and Flame* 157:1698–1717 (2010)